Gain-maximized GaAs/AlGaAs quantum-cascade laser with digitally graded active region

Indjin, D, Tomic, S, Ikonić, Z, Harrison, P, Kelsall, R.W., Milanović, V and Kočinac, S

http://dx.doi.org/10.1063/1.1508166

Gain-maximized GaAs/AlGaAs quantum-cascade laser with digitally graded active region

D. Indjin[a)]
School of Electronic and Electrical Engineering, University of Leeds, Leeds LS2 9JT, United Kingdom

S. Tomić
Department of Physics, University of Surrey, Guildford, Surrey GU2 7XH, United Kingdom

Z. Ikonić, P. Harrison, and R. W. Kelsall
School of Electronic and Electrical Engineering, University of Leeds, Leeds LS2 9JT, United Kingdom

V. Milanović
Faculty of Electrical Engineering, University of Belgrade, P.O. Box 35-54, 11120 Belgrade, Yugoslavia

S. Kočinac
Faculty of Technology and Metallurgy, University of Belgrade, 11000 Belgrade, Yugoslavia

(Received 2 May 2002; accepted for publication 27 July 2002)

An advanced strategy for the optimal design and realization of a GaAs/AlGaAs quantum-cascade laser is presented. It relies on recently established inverse scattering techniques to design an optimal smooth active region profile, followed by a conversion to an almost equivalent digitally graded structure, comprising just two different alloy compositions. In order to compare the output characteristics of optimized and previously realized structures, the intersubband electron scattering transport in quantum cascade lasers is analyzed. A full self-consistent rate equation model which includes all relevant electron-longitudinal optical phonon and electron–electron scattering mechanisms between injector/collector, active region, and continuumlike states is employed. Whilst the gain coefficients and threshold currents calculated at 77 and 300 K for the structure with a standard triple quantum well active region show excellent agreement with recent experiments, a significant improvement of these parameters is predicted for the optimized digitally graded quantum-cascade laser. © *2002 American Institute of Physics.* [DOI: 10.1063/1.1508166]

Following the first realization of intersubband transitions quantum-cascade lasers (QCLs)[1] significant progress has been made in the InGaAs/AlGaAs system.[2,3] More recently GaAs/AlGaAs QCLs have also been demonstrated[4] and considerable research effort[5–9] has resulted in the room-temperature pulsed-mode operation of a $GaAs/Al_{0.45}Ga_{0.55}As$ QCL with triple quantum well (TQW)[10] and superlattice[11] active region. The GaAs/AlGaAs system may also play a crucial role in lasing in the far-infrared range.[12–18]

Generally, the main task in the design of a QCL is to maximize the gain, by designing a suitable potential profile with the desired energy spectrum and wave functions, which determine the transition dipole moment(s) and transition rates, and eventually the gain. The charge transport in QCLs is mainly due to incoherent-scattering mechanisms,[19] and all principal scattering mechanisms, i.e., electron-longitudinal optical (LO) phonon and electron–electron, have to be included.[20,21] Because of the QCL complexity, the task of optimizing the whole structure in a single step is too involved. Instead, one can optimize the active region separately and, in the next step, add a properly designed injector/collector.

In contrast to the ''anticrossed-diagonal'' scheme of the TQW QCL active region,[4–9] in this letter, we propose an advanced strategy for the QCL optimal design and realization. It relies on recently established techniques for generating an optimal smooth quantum well profile by inverse spectral theory.[22,23] In the three-level QCL model with assumed unity-injection efficiency,[24] we define the figure of merit: $\Xi=(1-\tau_{64}/\tau_{96})\tau_9 z_{96}^2$, which depends directly on the active region profile, and is proportional to the modal gain. In our full 15-level model, the subscripts 9, 6, and 4 denote the upper, lower, and ground laser levels in the active region, respectively (Fig. 1), z_{96} is the optical dipole matrix element, τ_{ij} are the scattering times, and τ_9 the upper laser level lifetime. The maximization of gain, i.e., of the factor Ξ, may be accomplished by varying the profile of the active region in an isospectral manner,[22,23] which affects only the wave functions and not the state spacing. The procedure starts with an arbitrary initial potential and generates a family of potentials, which all have the required state spacings, their shape being controlled by a few parameters. In this case, we chose $\Delta E_{96}=132$ meV ($\lambda\approx 9.3\ \mu$m), $\Delta E_{64}=36$ meV (the LO phonon energy), and assumed a ''typical'' value of the electric field in a mid-infrared QCL of $F=48$ kV/cm, i.e., the corresponding linear potential is subtracted from the full potential in order to obtain the part to be realized by composition grading. The optimal active region profile with $z_{96}=2.9$ nm and $\Xi=690$ ps Å^2 is shown in the inset of Fig. 1.

A route toward an approximate realization of the optimal smooth potential is via digital grading (DG), using just two different alloy compositions to facilitate growth. The two compositions may be GaAs and $Al_{x_b}Ga_{1-x_b}As$, where x_b is

a)Electronic mail: d.indjin@ee.leeds.ac.uk

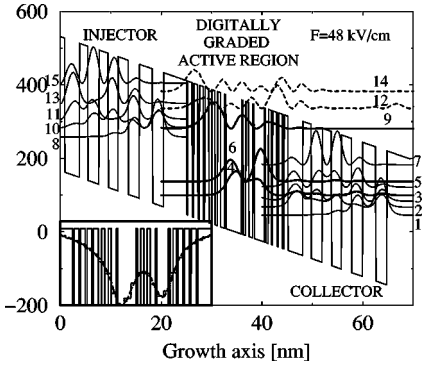

FIG. 1. A schematic diagram of quasibound energy levels and associated wave functions squared for 1 1/2 periods of DG GaAs/$Al_{0.44}Ga_{0.56}As$ QCL: injector (8, 10, 11, 13, and 15), active region (4, 6, and 9), collector (1, 2, 3, 5, and 7) and weakly localized-continuumlike (12 and 14) levels. The layer sequence of one period of structure, in nanometers, from the left- to the right-hand side starting from the injection barrier is **4.6**, 0.28, **0.84**, 0.28, **0.84**, 0.28, **0.84**, 0.28, **0.84**, 0.56, **0.56**, 0.56, **0.56**, 0.84, **0.28**, 3.08, **0.28**, 0.56, **0.56**, 0.84, **0.28**, 1.96, **0.28**, 0.56, **0.56**, 0.28, **0.84**, 0.28, **0.84**, 0.28, **0.84**, 2.88, **1.7**, 2.2, **1.8**, 2.0, **2.0**, 2.2, **2.6**, and 2.2. The normal script denotes the wells, bold script; the barriers, and underscore; the doped regions, with a nominal donor sheet density $N_s=3.9\times10^{11}$ cm^{-2}. The inset shows the structure of the DG active region, together with the optimal smooth potential and cell-averaged potential used in the DG design.

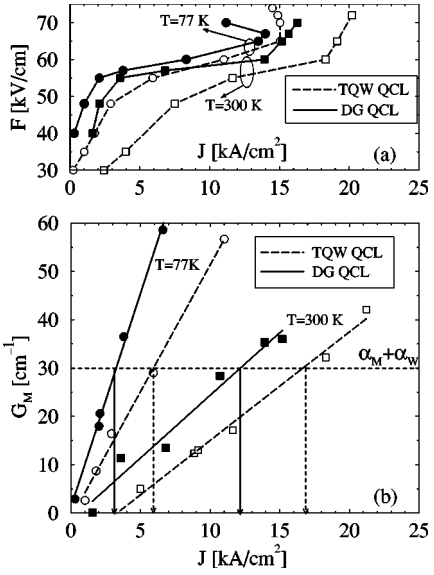

FIG. 2. (a) Electric field vs current density characteristics at $T=77$ K and $T=300$ K in DG QCL (solid lines) and TQW QCL (see Ref. 10) (dashed lines). (b) Calculated modal gain vs current density dependence at cryogenic and room temperatures for DG QCL (solid lines) and TQW QCL (see Ref. 10) (dashed lines). The symbols are the calculated results and the lines represent the least square fits used to derive the values of g. The horizontal dashed line denotes the total losses ($\alpha_M+\alpha_W\approx30$ cm^{-1}).

the Al mole fraction in the barriers of the smooth structure. DG has already been used for approximate realization of nonrectangular quantum wells (QWs).[25–27] To find the DG structure that best approximates an optimized smooth one, the latter is first divided into segments (''cells'') of width L_{cell}, with an integer multiple of crystalline monolayers (1 ml$\approx$2.83 Å). Depending on the average potential $\overline{U}(i)$ in ith cell, it is substituted by a well/barrier pair, their widths $L_w(i)$ and $L_b(i)$ being calculated as $L_b(i)/L_0=N_{\text{int}}[\overline{U}(i)L_{\text{cell}}/U_bL_0]$, and $L_w(i)=L_{\text{cell}}-L_b(i)$, where U_b is the potential of the barrier (the well is taken to be GaAs, so the potential $U_w=0$ therein), $L_0=2.83$ Å, and $N_{\text{int}}[\ldots]$ denotes the nearest integer value. The method in fact rounds the ''local'' potential to the nearest among the total of L_{cell} equispaced values, spanning the range between $U_w=0$ and U_b. Therefore, a small L_{cell} may imply a larger rounding error for a finely sampled potential, while large L_{cell} gives good reproduction of a coarsely sampled potential. In the design of the DG active region, we made a systematic search, with L_{cell} ranging from 2 to 12 ml. The best results were obtained with $L_{\text{cell}}=4$ ml and $x_b=0.44$, and the structure is described in the caption of Fig. 1. Values of $z_{96}=2.8$ nm and $\Xi=640$ ps Å^2 in a DG structure are quite near those in the optimal smooth one.[28]

In the next step, we designed a five QW injector/collector region, starting from the existing injector design[10] and modifying its parameters to match the new active region. An important issue is also a proper choice of the injection barrier[7] which couples the active and injector parts. Its choice is subject to the usual compromise between upper laser level confinement (i.e., large z_{96}), small leakage into continuum, and sufficient overlap with injector states, hence, rapid carrier transfer. In this process, we were guided by physical intuition relying on very careful inspection of wave functions and their overlap, because a formal optimization of electron–electron scattering based carrier relaxation and the Bragg confinement properties would be too involved. The layer sequence of the injector/collector is explained in the caption of Fig. 1.

In order to extract the output characteristic of the DG QCL beyond the three-level approximation and compare it with the recently realized GaAs/$Al_{0.45}Ga_{0.55}As$ TQW QCL,[10] we performed a full self-consistent rate equation modeling[16,29] of the electron scattering transport within the 15-level model of the QCL.[30] From the self-consistent solution, the population inversion $\Delta n_i=n_9-n_6$ in the steady state was obtained, and the modal gain was calculated from[24]

$$G_M=\frac{4\pi e^2}{\varepsilon_0 \underline{n}}\frac{z_{96}^2}{2\gamma_{96}L_p\lambda}\Gamma(n_9-n_6)\equiv g\Gamma J, \tag{1}$$

where λ is the laser emission wavelength, $2\gamma_{96}$ is the experimental linewidth, $\underline{n}$ is the mode refractive index, ε_0 is the vacuum dielectric permittivity, L_p is the length of one period (injector+active region), and Γ is the modal overlap factor. To extract the gain coefficient, one has to change the electric field (i.e. the applied voltage) and calculate the modal gain and total current density. The gain coefficient g [Eq. (1)] is then obtained from linear interpolation of $G_M(J)$. The threshold current density J_{th} is found from $G_M=g\Gamma J_{\text{th}}=\alpha_M+\alpha_W$, where α_M and α_W are the mirror and waveguide losses, respectively.

The calculated electric field–current density characteristics at 77 and 300 K for the DG QCL and TQW QCL[10] are similar, Fig. 2(a). A slower rise in the field at lower current densities in the DG QCL is due to a slightly larger injection barrier (effective) width therein, which is expected to decrease the $F(J)$ slope.[7] At 77 K in both structures, around 85% carriers in the injector populate its ground level 8, the rest being distributed over the upper levels (10, 11, 13, and 15). Current saturation and negative differential resistivity occur well above the threshold, when the field is high enough to misalign the ground injector and the upper laser states. At

room temperature, up to 50% of the carriers are found to populate the upper injector levels, hence, the smoother $J-F$ curve. The calculations for the TQW QCL are, thus, in good overall qualitative and quantitative agreement with experiment.[10]

Figure 2(b) shows the modal gain versus current density dependence for both QCLs at 77 and 300 K, calculated with $\lambda=9.3$ μm, $\underline{n}=3.28$, $L_p=45.3(45.0)$ nm, $2\gamma_{96}=12$ meV (at $T=77$ K), $2\gamma_{96}=22$ meV (at $T=300$ K).[10] Following Eq. (1), we can derive the gain coefficient g by dividing the slope of the linear fit by the overlap factor $\Gamma=0.42$.[4,8] For the TQW QCL, we obtain $g\approx11$ cm/kA at $T=77$ K and $g\approx5$ cm/kA at $T=300$ K. From the intersection points of the experimental[24] total loss line $\alpha_M+\alpha_W\approx30$ cm^{-1} and the $G_M(J)$ lines, for TQW QCL, we obtain the threshold current $J_{\text{th}}\approx6$ kA/cm^2 at $T=77$ K and $J_{\text{th}}\approx17$ kA/cm^2 at $T=300$ K. Both g and J_{th} for the TQW QCL are in very good agreement with experiment ($g=8.7$ cm/kA and $J_{\text{th}}=4-7$ kA/cm^2 at $T=77$ K, and $J_{\text{th}}=16-18$ kA/cm^2 at $T=300$ K).[4,8,10] The digitally optimized design shows a substantial improvement over the TQW QCL. The modal gain in the DG QCL is larger than that in TQW QCL for a range of current densities, with $g\approx21$ cm/kA at $T=77$ K and $g\approx6.5$ cm/kA at $T=300$ K. This leads to a significant reduction in threshold current, to $J_{\text{th}}\approx3$ kA/cm^2 at $T=77$ K, and $J_{\text{th}}\approx12$ kA/cm^2 at $T=300$ K. One may notice that the relative improvement in gain and reduction in threshold current provided by DG QCL at 300 K is not as large as at 77 K. This is because the somewhat wider active region DG QCL has slightly lower continuumlike states (12 and 14) and the lower laser level wave function (level 6) is shifted slightly downstream, as compared to the TQW QCL. Together with the fact that at higher temperatures the electrons populate higher injector/collector levels, causing larger leakage from the injector to the continuum and a larger backfilling from the collector to the active region, all these reduce the population inversion in the DG QCL. Yet, these effects are not excessive, and DG QCL retains the overall advantage over TQW QCL even at 300 K.

Finally, we briefly discuss some practical points in DG QCL realization. While the demand for very thin layers does not itself seem to be a problem for present technology, there may be some concern about the effects of layer width fluctuations and interface roughness. These cannot be simply quantified. Since the layers in the DG section are not confinement layers, but rather act via the average composition, with wave functions evenly penetrating the well and barrier slices, the width fluctuations should average out, with no significant effect on the wave function shapes. There is experimental evidence[31] that despite the increased number of interfaces the exitonic lines in such DG structures are not much broader than in simple rectangular QWs, so one may expect limited broadening of intersubband lines as well.

In summary, the procedure was described for design, realization, and numerical modeling of the carrier dynamics in gain optimized QCLs. Significant improvement of midinfrared QCL output characteristics is predicted. The DG optimal design principles may also be applied to terahertz QCLs, which are in the focus of current research.

The authors are grateful to J. W. Cockburn and L. R. Wilson, University of Sheffield, for useful discussions. This work is partially supported by EPSRC UK.

[1] J. Faist, F. Capasso, D. L. Sivco, A. L. Hutchinson, C. Sirtori, and A. Y. Cho, Science **264**, 553 (1994).
[2] For a recent review see C. Gmachl, F. Capasso, D. L. Sivco, and A. Y. Cho, Rep. Prog. Phys. **64**, 1533 (2001), and references therein.
[3] J. Faist, M. Beck, D. Hofstetter, and M. Rochat, *Proceedings of the SPIE Photonic West, San Jose, CA, 19–25 January 2002* (SPIE, Bellingham, WA, 2002), p. 113.
[4] C. Sirtori, P. Kruck, S. Barbieri, P. Collot, J. Nagle, M. Beck, J. Faist, and U. Oesterle, Appl. Phys. Lett. **73**, 3486 (1998).
[5] P. Kruck, H. Page, C. Sirtori, S. Barbieri, M. Stellmacher, and J. Nagle, Appl. Phys. Lett. **76**, 3340 (2000).
[6] C. Becker, C. Sirtori, H. Page, G. Glastre, V. Ortiz, X. Marcadet, M. Stellmacher, and J. Nagle, Appl. Phys. Lett. **77**, 463 (2000).
[7] S. Barbieri, C. Sirtori, H. Page, M. Stellmacher, and J. Nagle, Appl. Phys. Lett. **78**, 282 (2001).
[8] L. R. Wilson, P. T. Keightley, J. W. Cockburn, M. S. Skolnick, J. C. Clark, R. Grey, and G. Hill, Appl. Phys. Lett. **76**, 801 (2000).
[9] L. Hvozdara, A. Lugstein, N. Finger, S. Gianordoli, W. Schrenk, K. Unterrainer, E. Bertagnolli, G. Strasser, and E. Gornik, Appl. Phys. Lett. **77**, 1241 (2000).
[10] H. Page, C. Backer, A. Robertson, G. Glastre, V. Ortiz, and C. Sirtori, Appl. Phys. Lett. **78**, 3529 (2001).
[11] S. Anders, W. Schrenk, E. Gornik, and G. Strasser, Appl. Phys. Lett. **80**, 1864 (2002).
[12] M. Rochat, J. Faist, M. Beck, U. Oesterle, and M. Ilegems, Appl. Phys. Lett. **73**, 3724 (1998).
[13] R. Köhler, R. C. Iotti, A. Tredicucci, and F. Rossi, Appl. Phys. Lett. **79**, 3920 (2001).
[14] K. Donovan, P. Harrison, and R. W. Kelsall, Appl. Phys. Lett. **75**, 1999 (1999).
[15] R. Colombelli, A. Straub, F. Capasso, C. Gmachl, M. I. Blakey, A. M. Sergent, S. N. G. Chu, K. W. West, and L. N. Pfeiffer, J. Appl. Phys. **91**, 3526 (2002).
[16] P. Harrison and R. A. Soref, IEEE J. Quantum Electron. **37**, 153 (2001).
[17] R. Köhler, A. Tredicucci, F. Beltram, H. E. Beere, E. H. Linfield, A. G. Davies, and D. A. Ritchie, Appl. Phys. Lett. **80**, 1867 (2002).
[18] R. Köhler, A. Tredicucci, F. Beltram, H. E. Beere, E. H. Linfield, A. G. Davies, D. A. Ritchie, R. C. Iotti, and F. Rossi, Nature (London) **417**, 156 (2002).
[19] R. C. Iotti and F. Rossi, Phys. Rev. Lett. **87**, 144603-1 (2001).
[20] P. Harrison, *Quantum Wells, Wires, and Dots: Theoretical and Computational Physics* (Wiley, Chichester, 1999).
[21] P. Harrison, Appl. Phys. Lett. **75**, 2800 (1999).
[22] S. Tomić, M. Tadić, V. Milanović, and Z. Ikonić, J. Appl. Phys. **87**, 7965 (2000).
[23] S. Tomić, V. Milanović, and Z. Ikonić, IEEE J. Quantum Electron. **37**, 1337 (2001).
[24] S. Barbieri, C. Sirtori, H. Page, M. Back, J. Faist, and J. Nagle, IEEE J. Quantum Electron. **36**, 736 (2000).
[25] D. L. Mathine, G. N. Maracas, D. S. Gerber, R. Droopad, R. J. Graham, and M. R. McCartney, J. Appl. Phys. **75**, 4551 (1994).
[26] J. H. Lee, S. S. Li, M. Z. Tidrow, W. K. Liu, and K. Bacher, Appl. Phys. Lett. **75**, 3207 (1999).
[27] S. Vlaev, F. Garcia-Moliner, and V. R. Velasco, Phys. Rev. B **52**, 13784 (1995).
[28] The electron effective mass is $0.067m_0$ and $0.15m_0$ in GaAs and AlAs, and GaAs/AlAs conduction band offset is 836 meV. The Vegard's law is used for the alloy. Nonparabolicity was included, after C. Sirtori, F. Capasso, J. Faist, and S. Scandalo, Phys. Rev. B **50**, 8663 (1994).
[29] K. Donovan, P. Harrison, and R. W. Kelsall, J. Appl. Phys. **89**, 3084 (2001).
[30] D. Indjin, P. Harrison, R. W. Kelsall, and Z. Ikonić, J. Appl. Phys. **91**, 9019 (2002).
[31] W. Q. Chen, S. M. Wang, T. G. Andersson, and J. Thordson, Phys. Rev. B **48**, 14264 (1993).